MITSUBISHI ELECTRIC RESEARCH LABORATORIES
http://www.merl.com

Distributed Cyclic Delay Diversity Systems with Spatially Distributed Interferers

Kim, Kyeong Jin; Di Renzo, Marco; Liu, Hongwu; Tsiftsis, Theodoros A.; Orlik, Philip V.; Poor, H. Vincent

TR2019-162 December 24, 2019

Abstract

In this paper, a cooperative single carrier system comprising multiple cooperating remote radio heads (RRHs) and spatially distributed interferers is investigated. Due to the random location of the interferers within the communication range, a mixture of line-of-sight (LoS) and non-line-of-sight (nLoS) paths is considered in the channel model. Under a frequency selective fading channel with a mixture of the LoS and nLoS paths, the distributed cyclic delay diversity (dCDD) is employed to achieve the maximum transmit diversity gain without the exact knowledge of the channel state information at the transmitter side. It is shown that the operating signalto-noise (SNR) regions are divided in two regions, i.e., noiselimited and interference-limited. In this paper, the main focus is on the interference-limited region, in which diversity gain is not achieved due to performance limits determined by system and channel parameters. The existence of these limits on performance metrics, such as the outage probability and ergodic capacity is derived analytically, and then verified by link-level simulations.

IEEE Transactions on Wireless Communications

This work may not be copied or reproduced in whole or in part for any commercial purpose. Permission to copy in whole or in part without payment of fee is granted for nonprofit educational and research purposes provided that all such whole or partial copies include the following: a notice that such copying is by permission of Mitsubishi Electric Research Laboratories, Inc.; an acknowledgment of the authors and individual contributions to the work; and all applicable portions of the copyright notice. Copying, reproduction, or republishing for any other purpose shall require a license with payment of fee to Mitsubishi Electric Research Laboratories, Inc. All rights reserved.

Copyright © Mitsubishi Electric Research Laboratories, Inc., 2019
201 Broadway, Cambridge, Massachusetts 02139

Distributed Cyclic Delay Diversity Systems with Spatially Distributed Interferers

Kyeong Jin Kim, Marco Di Renzo, Hongwu Liu, Theodoros A. Tsiftsis,
Philip V. Orlik, and H. Vincent Poor

***Abstract*—In this paper, a cooperative single carrier system comprising multiple cooperating remote radio heads (RRHs) and spatially distributed interferers is investigated. Due to the random location of the interferers within the communication range, a mixture of line-of-sight (LoS) and non-line-of-sight (nLoS) paths is considered in the channel model. Under a frequency selective fading channel with a mixture of the LoS and nLoS paths, the distributed cyclic delay diversity (dCDD) is employed to achieve the maximum transmit diversity gain without the exact knowledge of the channel state information at the transmitter side. It is shown that the operating signal-to-noise (SNR) regions are divided in two regions, i.e., noise-limited and interference-limited. In this paper, the main focus is on the interference-limited region, in which diversity gain is not achieved due to performance limits determined by system and channel parameters. The existence of these limits on performance metrics, such as the outage probability and ergodic capacity is derived analytically, and then verified by link-level simulations.**

***Index Terms*—Distributed CDD, LoS and nLoS paths, cyclic-prefixed single carrier transmission, interferers, outage probability, ergodic capacity.**

I. Introduction

When channel state information (CSI) is available at the transmitter, several transmit diversity schemes such as maximum ratio transmission (MRT) [1]–[3], distributed space-time coding (STC) [4], and space-time block coding (STBC) [5] have been investigated. It is known that a full rate orthogonal STBC does not exist for a general number of distributed transmitters. For a general number of single antenna equipped transmitters, a distributed MRT was proposed by [3]. Although an increased signal-to-noise ratio (SNR) can be achieved by the use of MRT over independent channels, acquiring CSI is a challenging task in distributed systems. As one of the countermeasures, an asynchronous non-coherent joint transmission from base stations (BSs) or distributed transmitters are considered for orthogonal frequency division multiple access (OFDMA)-based wireless systems in [6] and [7]. Without a tight synchronization between BSs and transmitters, the same messages can be sent to the receiver.

K. J. Kim and P. V. Orlik are with Mitsubishi Electric Research Laboratories (MERL), Cambridge, MA, USA.

M. D. Renzo is with the Laboratoire des Signaux et Systèmes, CNRS, CentraleSupélec, Univ Paris Sud, Université Paris-Saclay, 3 rue Joliot Curie, Plateau du Moulon, 91192, Gif-sur-Yvette, France. (e-mail: marco.direnzo@l2s.centralesupelec.fr).

H. Liu is with Shandong Jiaotong University, Jinan, China.

T. A. Tsiftsis is with the School of Engineering, Nazarbayev University, Astana, Kazakhstan.

H. V. Poor is with the Department of Electrical Engineering, Princeton University, Princeton, NJ, USA.

As a more practical transmit diversity scheme, cyclic delay diversity (CDD) has been proposed, and has been widely used in practical orthogonal frequency division multiplexing (OFDM)-based wireless systems such as [8], [9], and [10]. CDD provides diversity benefits by enabling simultaneous multiple transmissions arriving at the CDD-receiver (CDD-RX), which combines the received signals with different cyclic delays. Without being aware of cyclic delays introduced by the transmitter, the CDD-RX can achieve diversity benefits. CDD introduces frequency selectivity in the considered cooperative wireless system, in which time variations due to the cyclic delay changes the frequency selectivity. Thus, the CDD scheme is based on the recognition that it improves the reliability of a message by transmitting over multiple communication channels having different channel characteristics. Although CDD requires a reduced complexity, in general, forward error correction (FEC) is also required to convert spatial diversity into frequency diversity.

Cyclic-prefixed single carrier (CP-SC) transmissions has been also proposed for several wireless systems [11] considering more practical issues such as peak-to-average ratio, power-backing off, and dynamic range of the linear amplifier [12]. For this transmissions, several works [13]–[16] have attempted to use CDD without considering of distributed CDD (dCDD). Only a recent work [17] proposes a dCDD scheme for a cooperative system with a set of spatially distributed single antenna equipped transmitters. Since dCDD converts the multiple-input and single-output channel into an intersymbol interference (ISI)-free single-input and single-output (SISO) channel, and this SISO channel is expressed by the right circulant matrix, two conditions are identified to make this channel matrix interference free from spatially distributed transmitters in frequency selective fading channels. Due to the ISI-free equivalent channel representation, the maximum diversity gain can be achieved from the channel and transmitter cooperation [17]. With the use of CP-SC transmissions, a full diversity gain can be achieved by using either best relaying selection [18] or best terminal selection [19]. However, only a single relay or user terminal (UT) is selected for transmission or reception, dCDD can provide a higher coding gain at the same full diversity gain, which overcomes the results of [14] that the full diversity gain is not achievable at a full transmission rate.

As a more realistic channel model, several works [20]–[23] consider a co-existence of line-of-sight (LoS) and non-line-of-sight (nLoS) paths between BSs and UT especially for mobile communications. In general, two and multi-slope path

loss models were employed. And then, a stochastic geometry analysis was developed to see the combined impact of LoS and nLoS paths on performance metrics for the new path loss models. As a distance between the BS and UT increases, a higher chance of nLoS path may exist [22]. Thus, a linear LoS probability function was adapted by 3GPP [23] to model the co-existence of LoS and nLoS paths. Since we assume that multiple interferers are uniformly distributed within the communications range of the considered cooperative system, we use a very similar path loss model between the CDD-RX and interferers [24]. Most of the recent works in [25] and [26] have mainly focused on coverage probability for a non cooperative system. In contrast, this paper considers dCDD-based transmit diversity, and specifies the spatially averaged signal-to-interference-plus-noise ratio (SA-SINR). Based on this new quantity, this paper analyzes the outage probability and ergodic capacity of the CP-SC system with dCDD in the frequency selective fading channel.

Utilizing the benefit of CP-SC transmissions, this paper investigates radio remote head (RRH) cooperation controlled by the control unit (CU). The CU controls RRHs either transmit the same information data to the CDD-RX over a frequency selective fading channel by assigning a different CDD delay to each RRHs or refrain from transmission if a RRH is not selected for CDD operation. The number of RRHs that apply CDD is limited due to construction of the ISI-free transmission, in which a fixed symbol block size and the maximum number of multipath components jointly determine the maximum CDD RRHs.

For this cooperative CP-SC system, we assume that multiple interferers are co-existed in the system. These interferers are assumed to be distributed uniformly and independently within the communications range, so that we adapt co-existing LoS and nLoS channels over the links from interferers to the CDD-RX. Since this paper assumes spatially distributed interferers, it is necessary to investigate the spatially averaged performance metrics.

Comparing with existing work, our main contributions are summarized as follows.

- We consider a finite-sized CP-SC system due to a limited number of RRHs for dCDD operation. With this restriction, it is necessary to use a mathematical analysis fit to finite-sized cooperative systems. However, in general, dCDD provides a better performance over other finite-sized cooperative systems [18], [19] that use only one opportunistically chosen node. For the considered system, we also investigate the impact of spatially distributed interferers on the performance metrics. However, the system model is not limited in terms of the number of RRHs and interferers. Any number of RRHs and interferers can be supported by the proposed system.
- We employ a channel model, which is somewhat similar to [20]–[23]. The co-existence of LoS and nLoS paths is modeled by using a fading time-share factor [24] that follows a binary Bernoulli process. The use of a new channel model for dCDD scheme is another difference from the work [17].
- We provide an analytical framework taking into account a different degree of RRH cooperation via dCDD, frequency selectivity, spatially distributed interference over the co-existing LoS and nLoS paths, in analyzing performance of the dCDD-based CP-SC system. For this new system, a new expression for the SA-SINR is derived. After then, its probability density function (PDF) and cumulative distribution function (CDF) are derived for the computation of the performance metrics. Although dCDD provides the maximum diversity with CP-SC transmissions in the interference-free scenario, it is an open problem to investigate the achievable diversity gain in the presence of a new type of interference. It is also an open problem to understand the effect of different degrees of LoS and nLoS path mixture on the diversity gain and ergodic capacity.
- We analyze the achievable diversity gain in noise and interference-limited regions separately. From this analysis, we derive the limits on the outage probability and ergodic capacity in the interference-limited region. For various system and channel parameters, we verify their accuracy from the link-level simulations. Although noise-limited and interference-limited regions are considered for the coverage probability analysis in [26], the system model is different from what we have investigated in this paper. In addition, [26] does not conduct performance analysis as this paper.

A. Organization

The rest of the paper is organized as follows. In Section II, we first detail the system and channel model of the dCDD-based CP-SC system. After defining random quantities and deriving their distributions, performance analysis of the considered system is conducted in Section III. Simulation results are presented in Section IV and conclusions are drawn in Section V.

B. Notation

$\mathbb{R}_+$ denotes the set of positive real numbers; $\mathbb{N}_0$ denotes the set of non-negative integers; $\mathbb{C}$ denotes the set of complex numbers; $\mathcal{CN}\left(\mu, \sigma^2\right)$ denotes the circularly symmetric complex Gaussian distribution with the mean μ and the variance σ^2; $B(a)$ denotes the binary Bernoulli process with a probability a; $F_{\varphi}(\cdot)$ and $f_{\varphi}(\cdot)$, respectively, denote the CDF and PDF of the random variable (RV) φ; $E\{\cdot\}$ denotes expectation. In addition, $\binom{n_1}{n_2} \triangleq \frac{n_1!}{n_2!(n_1-n_2)!}$ denotes the binomial coefficient. A length of a vector $\boldsymbol{a}$ is denoted by $\mathbb{L}(\boldsymbol{a})$; For a set of continuous random variables, $\{x_1, x_2, \ldots, x_N\}$, $x_{(i)}$ denotes the ith largest random variable.

II. System and Channel Model

A block diagram of the considered cooperative CP-SC system is provided in Fig. 1. We assume that a cooperative communication system comprising a controller or CU connected to M single antenna equipped RRHs, $\{\mathrm{RRH}_m\}_{m=1}^{M}$, via dedicated highly reliable backhaul connections, $\{b_m\}_{m=1}^{M}$,

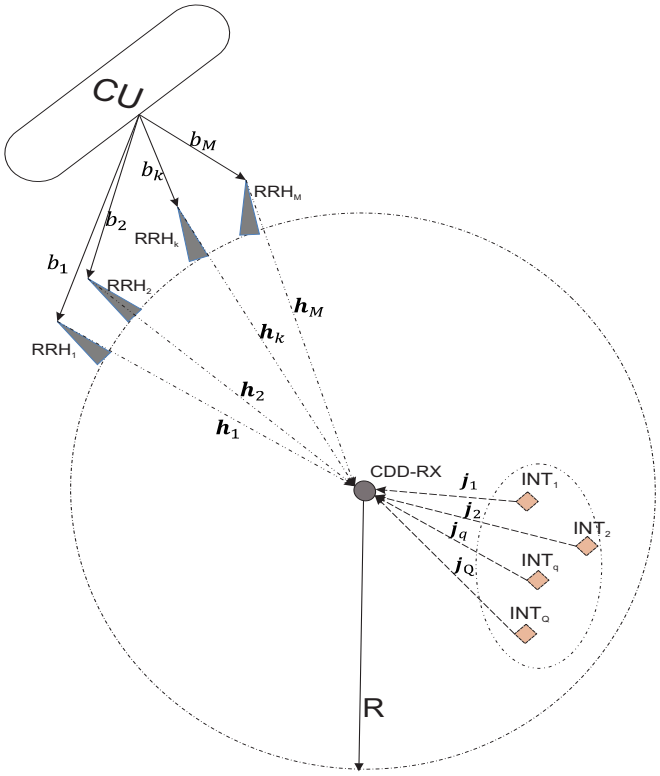

Fig. 1. Block diagram of the considered dCDD-based cooperative CP-SC system with spatially distributed interferers.

[7]. The CU forms an information data and controls RRHs to transmit the information data simultaneously using dCDD [17], so that any data decoding is not accomplished at the RRHs. A circular shaped communication range of radius R is formed around the single antenna equipped CDD-RX for cooperative communications between RRHs and CDD-RX with an aid from the CU, within which multiple single antenna equipped interferers (INTs) are spatially distributed uniformly and independently. To transmit the same information data from the RRHs, we assume that RRHs synchronize the operations by operating on a universal clock at the controller using signals from a Global Navigation Satellite System (GNSS) (e.g., GPS, Galileo, Glonass, QZSS, etc.). We also assume half-duplex transceivers, so that all the nodes are allowed to either send or receive data at a time. One of the unique features of dCDD is the integration of an RRH selection mechanism to achieve the diversity gain without requiring the exact channel state information at the transmitting side comprising the CU and RRHs. An investigation of its effect on the transmit diversity gain in the presence of a newly defined spatially distributed interference is the open question that we want to solve in this paper. To provide an insightful answer, we assume that RRHs are distributed at the same distance from the CDD-RX.

Compared with large-scale systems [20]–[22], this paper investigates only a finite-sized cooperative system comprising a fixed number of RRHs for the dCDD, and a fixed number of interferers. However, this system is scalable independent of the number of RRHs and interferers. Although many RRHs can support cooperative communications at a time, only a limited number of RRHs can be selected for dCDD to make interference free reception at the CDD-RX. This will be explained later.

Since RRH cooperation is usually optimized through channels connecting the CDD-RX, the set of frequency selective fading channels from the RRHs to the CDD-RX is assumed to be composed of LoS path, whereas the set of channels over the links from Q interferers to the CDD-RX is assumed to be comprising LoS and nLoS paths [20]–[23] due to their stochastic random location.

For the proposed system, we further assume the following channels and transmission schemes. By employing appropriate channel sounding scheme or channel reciprocity [27], [28], the CDD-RX is able to know the maximum number of multipath components over the channels from RRHs to the CDD-RX. Without specific description, we assume that the channel estimate is very reliable, and any impairment from the channel estimate is not considered. Thus, we do not make a distinction between actual channel and its estimate in the sequel.

A. Channels from RRHs to the CDD-RX

A multipath channel, $\boldsymbol{h}_k$, from the kth RRH to the CDD-RX is given by

$$\boldsymbol{h}_k = \sqrt{\alpha_{h,\mathrm{L}}}\tilde{\boldsymbol{h}}_{k,\mathrm{L}} \tag{1}$$

where $\tilde{\boldsymbol{h}}_{k,\mathrm{L}}$ denotes frequency selective fading for $\boldsymbol{h}_k$ with $N_h \triangleq \mathbb{L}(\tilde{\boldsymbol{h}}_{k,\mathrm{L}})$ multipath components. A distance-dependent path loss exponent is used to model large scale fading as $\alpha_{h,\mathrm{L}} = R^{-\epsilon_{\mathrm{L}}}$ with the LoS path loss exponent ϵ_{L} and distance R from the RRHs to CDD-RX. We assume that RRH cooperation is mainly accomplished in the presence of LoS channels. Due to an assumption that the RRHs are distributed at the same distance from the CDD-RX, we assume an independent and identically distributed (i.i.d.) frequency selective fading with an identical large scale fading across over the channels from the RRHs to CDD-RX.

B. Channels from interferers to the CDD-RX

A channel from the qth interferer to CDD-RX is given by

$$\boldsymbol{j}_q = \mathbb{I}_{j,\mathrm{L}}\sqrt{\alpha_{j_{q,\mathrm{L}}}}\tilde{\boldsymbol{j}}_{q,\mathrm{L}} + \mathbb{I}_{j,\mathrm{nL}}\sqrt{\alpha_{j_{q,\mathrm{nL}}}}\tilde{\boldsymbol{j}}_{q,\mathrm{nL}} \tag{2}$$

where $\tilde{\boldsymbol{j}}_{q,\mathrm{L}}$ and $\tilde{\boldsymbol{j}}_{q,\mathrm{nL}}$, respectively, identify frequency selective fading for LoS and nLoS paths with $(N_{j,\mathrm{L}})_q \triangleq \mathbb{L}(\tilde{\boldsymbol{j}}_{q,\mathrm{L}})$ and $(N_{j,\mathrm{nL}})_q \triangleq \mathbb{L}(\tilde{\boldsymbol{j}}_{q,\mathrm{nL}})$. In (2), complementary indicator functions $\mathbb{I}_{j,\mathrm{L}}$ and $\mathbb{I}_{j,\mathrm{nL}}$ are used to model co-existing LoS and nLoS by a time-share factor, $0 \le \mathcal{F} \le 1$, as follows:

$$\mathbb{I}_{j,\mathrm{nL}} \sim B(\mathcal{F}) \text{ and } \mathbb{I}_{j,\mathrm{L}} \triangleq 1 - \mathbb{I}_{j,\mathrm{nL}} \sim B(1-\mathcal{F}) \tag{3}$$

which specifies that for a fraction of time $\mathcal{F}$, a channel $\boldsymbol{j}_q$ introduces the nLoS path with a frequency selective fading, whereas for a fraction of time $1-\mathcal{F}$, a channel $\boldsymbol{j}_q$ introduces the LoS path with a frequency selective fading. A constant time-share for LoS and nLoS paths is assumed during transmissions over the channels from the interferers to CDD-RX. For large scale fading, we also assume that $\alpha_{j_{q,\mathrm{L}}} = (d_q)^{-\epsilon_{\mathrm{L}}}$ and $\alpha_{j_{q,\mathrm{nL}}} = (d_q)^{-\epsilon_{\mathrm{nL}}}$ for distance $d_q \in (0, R)$ from the qth interferer to the CDD-RX.

C. dCDD for CP-SC Transmissions

Different number of multipath components is more realistic. However, its relevant closed-form expressions for the performance metrics do not exist, in general. Also, this paper mainly investigates foundational insights into the dCDD performance in the presence of the interferers. From these reasons, we assume i.i.d. frequency selective fading channels from the interferers to CDD-RX.

We also assume that single carrier transmissions with the use of the cyclic prefix[1] [18] are used by every nodes in the system. To remove ISI due to a multipath channel, the last N_p modulation symbols from a transmission symbol block $\boldsymbol{s} \in \mathbb{C}^{B\times 1}$ are appended to the front of $\boldsymbol{s}$ [17]. The size of the transmission symbol block $\boldsymbol{s}$ is denoted by B. We assume that $E\{\boldsymbol{s}\} = \boldsymbol{0}$ and $E\{\|\boldsymbol{s}\|^2\} = \boldsymbol{I}_B$. According to [17], dCDD is a transmit diversity scheme that converts the multiple-input and single-output (MISO) channels into the SISO channels for CP-SC transmissions [16]. To make an ISI-free right circulant channel matrix, the CP length, N_p, and the ith CDD delay, Δ_i, need to be designed efficiently by the following two conditions [17]:

$$N_p \geq N_h, \tag{4}$$

$$\Delta_i = (i-1)N_p. \tag{5}$$

Based on (4) and (5), the maximum allowable number of RRHs for dCDD operation is determined by

$$K = \left\lfloor \frac{B}{N_p} \right\rfloor \tag{6}$$

where $\lfloor \cdot \rfloor$ denotes the floor function.

Since we assume $M \geq K$ RRHs in the considered system, the CU needs to select only K CDD RRHs[2]. A detailed description about RRH selection with its accompanying interactive operation between the CCD-RX and CU for dCDD operation is available in [17], so that we do not provide it in this paper. In summary, we can achieve the maximum diversity gain without explicit CSI feeding back from the CDD-RX to the CU and RRHs. That is, the employed dCDD operation allows the distributed cooperative system to achieve transmit diversity without requiring CSI at the CU and RRHs.

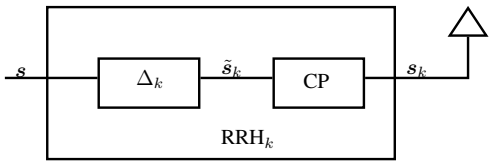

Fig. 2. Block diagram of dCDD operation at the kth RRH, RRH$_k$.

[1]Interested readers can find several advantages of CP-SC transmissions over OFDM transmissions from [12].

[2]Due to the employed RRH selection mechanism, the order statistics are involved in the representations of the received signals. However, when $M \leq K$, it is not necessary to employ the order statistics.

Due to dCDD operation, the received signal at the CDD-RX, after removing the CP signal, is given by

$$\boldsymbol{r} = \sqrt{P_s \alpha_{h,\mathrm{L}}} \sum_{k=1}^{K} \tilde{\boldsymbol{H}}_{(M-K+k),\mathrm{L}} \underbrace{\boldsymbol{P}_B^{\Delta_k} \boldsymbol{s}}_{\triangleq\ \tilde{\boldsymbol{s}}_k} + \sqrt{P_J} \sum_{q=1}^{Q} \boldsymbol{J}_q \boldsymbol{x}_{J,q} + \boldsymbol{z}_R \tag{7}$$

where the transmission power allocated at all the RRHs is P_s, $\tilde{\boldsymbol{H}}_{(M-K+k),\mathrm{L}}$ is the right circulant matrix specified by the $(M-K+k)$th LoS channel $\tilde{\boldsymbol{h}}_{(M-K+k),\mathrm{L}}$ and $\boldsymbol{P}_B^{\Delta_k}$ is the permutation shifting matrix[3], which is obtained from the identity matrix $\boldsymbol{I}_B$ by circularly shifting down by Δ_k. The additive noise over the desired channels is denoted by $\boldsymbol{z}_R \sim \mathcal{CN}(\boldsymbol{0}, \sigma_z^2 \boldsymbol{I}_B)$. Since the CU prevents non-selected RRHs from transmissions for dCDD operation, the CDD-RX does not experience interference from non-selected RRHs, whereas Q interferers interfere the CDD-RX since they are not controlled by the CU. Similar to the type of $\tilde{\boldsymbol{H}}_{(M-K+k),\mathrm{L}}$, $\boldsymbol{J}_q$ is also a right circulant matrix which is mainly specified by $\boldsymbol{j}_q$. Interfering symbol block from the qth interferer is given by $\boldsymbol{x}_{J,q}$ with $E\{\boldsymbol{x}_{J,q}\} = \boldsymbol{0}$ and $E\{\boldsymbol{x}_{J,q}\boldsymbol{x}_{J,q}^H\} = \boldsymbol{I}_B, \forall q$. The transmission power allocated to the all interferers is denoted by P_J.

Further by applying (4) and (5), (7) can be rewritten as follows:

$$\boldsymbol{r} = \boldsymbol{H}_{\mathrm{CDD}} \boldsymbol{s} + \sqrt{P_J} \sum_{q=1}^{Q} \boldsymbol{J}_q \boldsymbol{x}_{J,q} + \boldsymbol{z}_R \tag{8}$$

where $\boldsymbol{H}^{\mathrm{CDD}}$ is an equivalent channel matrix comprising the frequency fading channels from the K CDD RRHs to CDD-RX. Its first column vector is specified as follows:

$$\begin{aligned} \boldsymbol{h}^{\mathrm{CDD}} \triangleq\ & \sqrt{P_s \alpha_{h,\mathrm{L}}} \Big[(\tilde{\boldsymbol{h}}_{(M-K+1),\mathrm{L}})^T, \boldsymbol{0}_{1\times(N_{\max}-N_h)}, \\ & (\tilde{\boldsymbol{h}}_{(M-K+2),\mathrm{L}})^T, \boldsymbol{0}_{1\times(N_{\max}-N_h)}, \ldots, \\ & (\tilde{\boldsymbol{h}}_{(M),\mathrm{L}})^T, \boldsymbol{0}_{1\times(N_{\max}-N_h)} \Big]^T \in \mathbb{C}^{B\times 1} \end{aligned} \tag{9}$$

which shows an ISI-free equivalent channel vector composed by K independent channels. By specifying $\boldsymbol{h}^{\mathrm{CDD}}$, an equivalent channel matrix $\boldsymbol{H}_{\mathrm{CDD}}$ can be exactly determined.

III. Performance Analysis

From (7) and (8), the signal-to-interference-plus-noise ratio (SINR) is given by

$$\begin{aligned} \gamma_{\mathrm{SINR}} &\triangleq \frac{P_s \alpha_{h,\mathrm{L}} \sum_{k=1}^{K} \|\tilde{\boldsymbol{h}}_{(M-K+k),\mathrm{L}}\|^2}{P_J \sum_{q=1}^{Q} \|\boldsymbol{j}_q\|^2 + \sigma_z^2} \\ &= \frac{P_s \tilde{\alpha}_{h,\mathrm{L}} \sum_{k=1}^{K} \|\tilde{\boldsymbol{h}}_{(M-K+k),\mathrm{L}}\|^2}{\tilde{P}_J \sum_{q=1}^{Q} \|\boldsymbol{j}_q\|^2 + 1} \\ &= \frac{S}{J+1} \end{aligned} \tag{10}$$

[3]To achieve an ISI-free right circulant matrix, $\boldsymbol{P}_B^{\Delta_k}$ also needs to be right circulant, which makes the product of two matrices $\tilde{\boldsymbol{H}}_{(M-K+k),\mathrm{L}} \boldsymbol{P}_B^{\Delta_k}$ right circulant.

where $\tilde{\alpha}_{h,\mathrm{L}} \triangleq \frac{\alpha_{h,\mathrm{L}}}{\sigma_z^2}$, $S \triangleq P_s\tilde{\alpha}_{h,\mathrm{L}}\sum_{k=1}^{K}\|\tilde{\boldsymbol{h}}_{(M-K+k),\mathrm{L}}\|^2$, $\tilde{P}_J \triangleq \frac{P_J}{\sigma_z^2}$, and $J \triangleq \tilde{P}_J\sum_{q=1}^{Q}\|\boldsymbol{j}_q\|^2$. Note that by using the QRD-M detector [29], [30], we can obtain (10).

To understand the statistical properties of the SINR, we need to prepare the distributions of a channel power, co-existing with LoS and nLoS paths.

A. Distributions relevant to co-existing LoS and nLoS paths

We first derive the distribution of the interfering channel power in the following Proposition.

Proposition 1: Due to co-existing independent LoS and nLoS paths, the power of a particular interfering channel, $J_q \triangleq \|\boldsymbol{j}_q\|^2$, has the CDF as follows:

$$F_{J_q}(x) = (1-\mathcal{F})F_{\alpha_{j_{q,\mathrm{L}}}\|\tilde{\boldsymbol{j}}_{q,\mathrm{L}}\|^2}(x) + \mathcal{F}F_{\alpha_{j_{q,\mathrm{nL}}}\|\tilde{\boldsymbol{j}}_{q,\mathrm{nL}}\|^2}(x) \quad (11)$$

where $F_{\alpha_{j_{q,\mathrm{L}}}\|\tilde{\boldsymbol{j}}_{q,\mathrm{L}}\|^2}(x)$ and $F_{\alpha_{j_{q,\mathrm{nL}}}\|\tilde{\boldsymbol{j}}_{q,\mathrm{nL}}\|^2}(x)$ are, respectively, CDFs of $\alpha_{j_{q,\mathrm{L}}}\|\tilde{\boldsymbol{j}}_{q,\mathrm{L}}\|^2$ and $\alpha_{j_{q,\mathrm{nL}}}\|\tilde{\boldsymbol{j}}_{q,\mathrm{nL}}\|^2$.

Proof: Using the properties of binary Bernoulli process, we can easily verify (11). ∎

For frequency selective fading channels, the CDF of J_q can be expressed as

$$F_{J_q}(x) = (1-\mathcal{F})\left(1 - e^{-x/\alpha_{j_{q,\mathrm{L}}}}\sum_{l=0}^{(N_{j,\mathrm{L}})_q-1}\frac{1}{l!}\left(\frac{x}{\alpha_{j_{q,\mathrm{L}}}}\right)^l\right) + \mathcal{F}\left(1 - e^{-x/\alpha_{j_{q,\mathrm{nL}}}}\sum_{l=0}^{(N_{j,\mathrm{nL}})_q}\frac{1}{l!}\left(\frac{x}{\alpha_{j_{q,\mathrm{nL}}}}\right)^l\right). \quad (12)$$

Similarly, having applied the i.i.d. frequency selective fading channel assumption, we can have the CDF of J as

$$F_J(x) = 1-(1-\mathcal{F})\left(e^{-x/\tilde{P}_J\alpha_{j_{,\mathrm{L}}}}\sum_{l=0}^{QN_{j,\mathrm{L}}-1}\frac{1}{l!}\left(\frac{x}{\tilde{P}_J\alpha_{j_{,\mathrm{L}}}}\right)^l\right) + \mathcal{F}\left(e^{-x/\tilde{P}_J\alpha_{j_{,\mathrm{nL}}}}\sum_{l=0}^{QN_{j,\mathrm{nL}}}\frac{1}{l!}\left(\frac{x}{\tilde{P}_J\alpha_{j_{,\mathrm{nL}}}}\right)^l\right). \quad (13)$$

B. Distributions of the SA-SINR

To compute the distributions of the SA-SINR over the interferers placed at random within the communication range, we define the following quantities:

$$\mathbb{X} \triangleq \left\{\mathbb{X}_j \triangleq \{\boldsymbol{j}_q\}_{q=1}^{Q}, \mathbb{A}_j \triangleq \{\alpha_{j_{,\mathrm{L}}}, \alpha_{j_{,\mathrm{nL}}}\}\right\} \quad (14)$$

which denotes the set of small and large scale fading over the channels from Q interferers to the CDD-RX.

The CDF of the γ_{SINR}, $F_{\gamma_{\mathrm{SINR}}}(x)$, is given by

$$\begin{aligned} F_{\gamma_{\mathrm{SINR}}}(x) &= Pr(\gamma_{\mathrm{SINR}} < x) = E_{\mathbb{X}}\{F_S((J+1)x|J)\} \\ &= E_{\mathbb{A}_j}\{E_{\mathbb{X}_j}\{F_S((J+1)x|\mathbb{A}_j)\}\}, \end{aligned} \quad (15)$$

where $F_S((J+1)x|\mathbb{A}_j)$ is the conditional CDF, from which we can derive the desired CDF of the γ_{SINR}. According to [17], $F_S((J+1)x|\mathbb{A}_j)$ is given by

$$F_S(x(J+1)) = 1-\Psi(M,K,N_h)\left[\frac{B_1}{\Gamma(f)}\Gamma_u\left(f,\frac{(J+1)x}{\tilde{\alpha}_h}\right) + \frac{B_2}{\Gamma(f)}\Gamma_u\left(f,\frac{(J+1)x}{\beta\tilde{\alpha}_h}\right)\right] \quad (16)$$

where $\Gamma(\cdot)$ and $\Gamma_u(\cdot,\cdot)$ denote the complete gamma and upper incomplete gamma functions, respectively, and others terms are defined at the top of the next pages. In (16), we have defined $\beta \triangleq \frac{K}{1+p+K}$, $m_1 \triangleq N_hK-\tilde{l}$, $m_2 \triangleq \tilde{l}+\tilde{q}+N_h$, $\tilde{q} \triangleq \sum_{t=0}^{N_h-1}tq_{t+1}$ for a non-negative integer set $\{q_1,q_2,\ldots,q_{N_h}\}$ satisfying the condition $\sum_{k=1}^{N_h}q_k = p$ and $\tilde{l} \triangleq \sum_{t=0}^{N_h-1}tl_{t+1}$ for another non-negative integer set $\{l_1,l_2,\ldots,l_{N_h}\}$ satisfying the condition $\sum_{k=1}^{N_h}l_k = K$.

Now using $F_S\big((J+1)x|\mathbb{A}_j\big)$, and the set of frequency selective fading channels $\{\boldsymbol{j}_q\}_{q=1}^{Q}$, the SA-CDF of the γ_{SINR} achievable by the employed dCDD in the presence of spatially distributed interferers is provided in the following theorem.

Theorem 1: The SA-CDF of the SINR in i.i.d. frequency selective fading channels is given by (18) at the next pages.

Proof: See appendix A. ∎

In (18), ${}_2F_1(\cdot,\cdot,\cdot,\cdot)$ denotes the Gauss hypergeometric function [31, eq. (9.111)]. In addition, we have defined $N_{j,1} \triangleq QN_{j,\mathrm{L}}$, $N_{j,2} \triangleq QN_{j,\mathrm{nL}}$, $w_1 \triangleq w+QN_{j,\mathrm{L}}$, $w_2 \triangleq w+QN_{j,\mathrm{nL}}$, $f_{a,1} \triangleq QN_{j,\mathrm{L}}+2/\epsilon_{\mathrm{L}}$, $f_{a,2} \triangleq QN_{j,\mathrm{nL}}+2/\epsilon_{\mathrm{nL}}$, $f_{c,1} \triangleq QN_{j,\mathrm{L}}+2/\epsilon_{\mathrm{L}}+1$, $f_{c,2} \triangleq QN_{j,\mathrm{nL}}+2/\epsilon_{\mathrm{nL}}+1$, $f_{f,1} \triangleq \frac{\tilde{P}_J}{R^{\epsilon_{\mathrm{L}}}\tilde{\alpha}_h}$, $f_{f,2} \triangleq \frac{\tilde{P}_J}{R^{\epsilon_{\mathrm{nL}}}\tilde{\alpha}_h}$, $f_{f,3} \triangleq \frac{\tilde{P}_J}{R^{\epsilon_{\mathrm{L}}}\beta\tilde{\alpha}_h}$, and $f_{f,4} \triangleq \frac{\tilde{P}_J}{R^{\epsilon_{\mathrm{nL}}}\beta\tilde{\alpha}_h}$.

Note that *Theorem 1* provides a general analytical framework considering a time share factor $\mathcal{F}$ for LoS and nLoS paths due to stochastic random location of the interferers within the communication range. Thus, this new expression for the CDF of the SA-SINR can be used for a wide range of scenarios with frequency selective fading channels, arbitrary-degree of RRH cooperation via dCCD operation, time-share factor for LoS and nLoS paths, number of interferers, interference power, and size of communication range. This theorem also shows that the CDF of the SA-SINR is expressed by the sum of the Gauss hypergeometric functions.

C. Outage Probability and diversity gain analysis

From (10), two regions can be distinguishable depending on the magnitude of J.

1) Noise-Limited Region: When $J \ll 1$, an influence of interference compared with that of the noise can be negligible, so that the outage probability at a particular value, o_{th}, that is causing the outage, is given by

$$P_{\mathrm{ouage}}^{\mathrm{NL}}(o_{\mathrm{th}}) = F_s(o_{\mathrm{th}}). \quad (19)$$

It was proven by [17] that the maximum diversity gain can be achievable with

$$G_d = MN_h. \quad (20)$$

That is, the number of multipath elements over the desired channels from the RRHs to CDD-RX and the total number of RRHs in the system determine the diversity gain. Note that a cell association scheme is proposed in [26] which uses

$$\Psi(M,K,N_h) \triangleq \frac{M}{\Gamma(N_h)}\binom{M-1}{K}\sum_{p=0}^{M-K-1}\binom{M-K-1}{p}(-1)^p \sum_{\substack{q_1,\ldots,q_{N_h}\\ q_1+q_2+\ldots+q_{N_h}=p}}\frac{p!}{q_1!q_2!\ldots q_{N_h}!}$$
$$\sum_{\substack{l_1,\ldots,l_{N_h}\\ l_1+\ldots+l_{N_h}=K}}\frac{K!}{l_1!l_2!\ldots l_{N_h}!}\prod_{t_1=0}^{N_h-1}\Big(\frac{1}{t_1!}\Big)^{q_{t_1+1}}\prod_{t_2=0}^{N_h-1}\Big(\frac{1}{t_2!}\Big)^{l_{t_2+1}}\Gamma(\tilde{l}+\tilde{q}+N_h)$$
$$(1+p+K)^{-\tilde{l}-\tilde{q}-N_h},$$
$$B_1 \triangleq \sum_{f=1}^{m_1}(-1)^{m_1-f}\beta^{m_1-f}(1-\beta)^{-m_1-m_2+f}\binom{m_1+m_2-f-1}{m_1-f}, \text{ and}$$
$$B_2 \triangleq \sum_{f=1}^{m_2}(-1)^{m_2-f}\beta^{m_1-f}(\beta-1)^{-m_1-m_2+f}\beta^{f}\binom{m_1+m_2-f-1}{m_2-f}. \tag{17}$$

$$F_{\gamma_{\text{SINR}}}(x) = 1-\Psi(M,K,N_h)\Bigg[\sum_{l_a=0}^{f-1}\frac{B_1 x^{l_a}e^{-x/\tilde{\alpha}_h}}{\Gamma(l_a+1)(\tilde{\alpha}_h)^{l_a}}\sum_{w=0}^{l_a}\binom{l_a}{w}\Bigg[\frac{(1-\mathcal{F})\Gamma(w_1)}{\Gamma(N_{j,1})(\tilde{P}_J)^{N_{j,1}}}\frac{2R^{\epsilon_{\text{L}}N_{j,1}}}{\epsilon_{\text{L}}f_{a,1}}\Big(\frac{x}{\tilde{\alpha}_h}\Big)^{-w_1}$$
$${}_2F_1\Big(f_{a,1},w_1;f_{c,1};-1/(f_{f,1}x)\Big)+\frac{\mathcal{F}\Gamma(w_2)}{\Gamma(N_{j,2})(\tilde{P}_J)^{N_{j,2}}}\frac{2R^{\epsilon_{\text{nL}}N_{j,2}}}{\epsilon_{\text{nL}}f_{a,2}}\Big(\frac{x}{\tilde{\alpha}_h}\Big)^{-w_2}$$
$${}_2F_1\Big(f_{a,2},w_2;f_{c,2};-1/(f_{f,2}x)\Big)\Bigg]+\sum_{l_a=0}^{f-1}\frac{B_2 x^{l_a}e^{-\frac{x}{\tilde{\alpha}_h}}}{\Gamma(l_a+1)(\beta\tilde{\alpha}_h)^{la}}\sum_{w=0}^{l_a}\binom{l_a}{w}\Bigg[\frac{(1-\mathcal{F})\Gamma(w_1)}{\Gamma(N_{j,1})(\tilde{P}_J)^{N_{j,1}}}\frac{2R^{\epsilon_{\text{L}}N_{j,1}}}{\epsilon_{\text{L}}f_{a,1}}\Big(\frac{x}{\beta\tilde{\alpha}_h}\Big)^{-w_1}$$
$${}_2F_1\Big(f_{a,1},w_1;f_{c,1};-1/(f_{f,3}x)\Big)+\frac{\mathcal{F}\Gamma(w_2)}{\Gamma(N_{j,2})(\tilde{P}_J)^{N_{j,2}}}\frac{2R^{\epsilon_{\text{nL}}N_{j,2}}}{\epsilon_{\text{nL}}f_{a,2}}\Big(\frac{x}{\beta\tilde{\alpha}_h}\Big)^{-w_2}$$
$${}_2F_1\Big(f_{a,2},w_2;f_{c,2};-1/(f_{f,4}x)\Big)\Bigg]\Bigg]$$
$$=1-\tilde{F}_{\gamma_{\text{SINR}}}(x). \tag{18}$$

either the strongest average received power or the strongest instantaneous SINR. This is the case with $K=1$ of the dCDD scheme. Thus, when the proposed dCDD is utilized in the cell association, then a higher coverage probability can be obtained.

2) Interference-Limited Region: In this region, the influence of interference is larger than that of the noise, so that (10) can be approximated as follows:

$$\gamma_{\text{SINR}} \triangleq \frac{P_s\alpha_{h,\text{L}}\sum_{k=1}^{K}\|\tilde{\boldsymbol{h}}_{(M-K+k),\text{L}}\|^2}{P_J\sum_{q=1}^{Q}\|\boldsymbol{j}_q\|^2+\sigma_z^2} \approx \frac{P_s\alpha_{h,\text{L}}\sum_{k=1}^{K}\|\tilde{\boldsymbol{h}}_{(M-K+k),\text{L}}\|^2}{P_J\sum_{q=1}^{Q}\|\boldsymbol{j}_q\|^2} \tag{21}$$

which shows that diversity gain cannot be achievable when P_J is fixed independent of the noise power. Thus, we can summarize the achievable diversity gain in the following corollary.

Corollary 1: In the interference-limited region, the asymptotic outage probability floor limits the asymptotic outage probability, and is given by (22) at the top of the next page.

Proof: This can be readily obtained from *Theorem 1*. ■

Although ${}_2F_1\big(a_1,a_2;b_1;z\big)\overset{z\to\infty}{\propto}z^{-\min(a_1,a_2)}$, it is not able to be used in the interference-limited region due to a fixed argument of z in (22). However, we can see that $P_{\text{outage}}^{\text{IL}}(o_{\text{th}})$ has no dependency on the noise power in the expression, so that this corollary verifies that the dCDD-based CP-SC system cannot achieve the diversity gain in the interference-limited region, whereas it is achievable only in the noise-limited region. Parameters, such as the degrees of RRH cooperation, number of multipath components, number of interferers, interference power, time-share factor for LoS and nLoS paths, interference power, size of the communication range, and pathloss exponent jointly determine the floor on the outage probability.

D. Generalized Bivariate Meijer G-function

For the following set of parameters

$$\mathbb{X}_a \triangleq [a_1,\ldots,a_{p_1}],\mathbb{X}_b \triangleq [b_1,\ldots,b_{q_1}],$$
$$\mathbb{X}_c \triangleq [c_1,\ldots,c_{p_2}],\mathbb{X}_d \triangleq [d_1,\ldots,d_{q_2}],$$
$$\mathbb{X}_e \triangleq [e_1,\ldots,e_{p_3}], \text{ and } \mathbb{X}_f \triangleq [f_1,\ldots,f_{q_3}] \tag{23}$$

we define the generalized bivariate Meijer G-function [32, eq. (07.34.21.0081.01)] and [33] provided in (24) at the next page.

$$P_{\text{outage}}^{\text{IL}}(o_{\text{th}}) = 1 - \Psi(M,K,N_h)\Bigg[\sum_{l_a=0}^{f-1}\frac{B_1}{\Gamma(l_a+1)}\Bigg[\frac{(1-\mathcal{F})\Gamma(l_a+N_{j,1})}{\Gamma(N_{j,1})(P_J)^{N_{j,1}}}\frac{2R^{\epsilon_{\text{L}}N_{j,1}}}{\epsilon_{\text{L}}N_{j,1}+2}\Big(\frac{o_{\text{th}}}{\alpha_h}\Big)^{-N_{j,1}}$$
$${}_2F_1\Big(f_{a,1},l_a+N_{j,1};f_{c,1};-1/(f_{f,1}o_{\text{th}})\Big)+\frac{\mathcal{F}\Gamma(l_a+N_{j,2})}{\Gamma(N_{j,2})(P_J)^{N_{j,2}}}\frac{2R^{\epsilon_{\text{nL}}N_{j,2}}}{\epsilon_{\text{nL}}N_{j,2}+2}\Big(\frac{o_{\text{th}}}{\tilde{\alpha}_h}\Big)^{-N_{j,2}}$$
$${}_2F_1\Big(f_{a,2},l_a+N_{j,2};f_{c,2};-1/(f_{f,2}o_{\text{th}})\Big)\Bigg]+\sum_{l_a=0}^{f-1}\frac{B_2}{\Gamma(l_a+1)}\Bigg[\frac{(1-\mathcal{F})\Gamma(l_a+N_{j,1})}{\Gamma(N_{j,1})(P_J)^{N_{j,1}}}\frac{2R^{\epsilon_{\text{L}}N_{j,1}}}{\epsilon_{\text{L}}N_{j,1}+2}\Big(\frac{o_{\text{th}}}{\beta\alpha_h}\Big)^{-N_{j,1}}$$
$${}_2F_1\Big(f_{a,1},l_a+N_{j,1};f_{c,1};-1/(f_{f,3}o_{\text{th}})\Big)+\frac{\mathcal{F}\Gamma(l_a+N_{j,2})}{\Gamma(N_{j,2})(P_J)^{N_{j,2}}}\frac{2R^{\epsilon_{\text{nL}}N_{j,2}}}{\epsilon_{\text{nL}}N_{j,2}+2}\Big(\frac{o_{\text{th}}}{\beta\alpha_h}\Big)^{-N_{j,2}}$$
$${}_2F_1\Big(f_{a,2},l_a+N_{j,2};f_{c,2};-1/(f_{f,4}o_{\text{th}})\Big)\Bigg]\Bigg]. \tag{22}$$

$$G_{p_1,q_1:p_2,q_2:p_3,q_3}^{m_1,0:m_2,n_2:m_3:n_3}\Big(x,y\Big|\begin{array}{c|c|c}\mathbb{X}_a & \mathbb{X}_c & \mathbb{X}_e\\ \mathbb{X}_b & \mathbb{X}_d & \mathbb{X}_f\end{array}\Big) =$$
$$\frac{1}{(2\pi i)^2}\int_{L_1}\int_{L_2}\frac{\prod_{j=1}^{m_1}\Gamma(a_j+s+t)\prod_{j=1}^{m_2}\Gamma(1-c_j+s)\prod_{j=1}^{n_2}\Gamma(d_j-s)}{\prod_{j=m_1+1}^{p_1}\Gamma(1-a_j-s-t)\prod_{j=1}^{q_1}\Gamma(b_j+s+t)\prod_{j=m_2+1}^{p_2}\Gamma(c_j-s)}$$
$$\frac{\prod_{j=1}^{m_3}\Gamma(1-e_j+t)\prod_{j=1}^{n_3}\Gamma(f_j-t)}{\prod_{j=n_2+1}^{q_2}\Gamma(1-d_j+s)\prod_{j=m_3+1}^{p_3}\Gamma(e_j-t)\prod_{j=n_3+1}^{q_3}\Gamma(1-f_j+t)}x^s y^t \mathrm{d}s\mathrm{d}t. \tag{24}$$

In (24), L_1 and L_2 are contours in the s-plane and t-plane, respectively. Using either available Mathematica or Matlab codes in [33, Table II] and [34], respectively, it is possible to get an analytic performance for a set of particular system parameters. However, since the Mathematica code available in [33, Table II] is not working for all the system parameters, we have updated its closed contours L_1 and L_2 based on those specified in [34]. This provides a reliable generalized bivariate Meijer G-function for all the considered simulation cases.

E. Ergodic Capacity

Using (18), the ergodic capacity is defined by [35]

$$C = \frac{1}{\log(2)}\int_0^\infty \frac{1-F_{\gamma_{\text{SINR}}}(x)}{1+x}dx = \frac{1}{\log(2)}\int_0^\infty \frac{\tilde{F}_{\gamma_{\text{SINR}}}(x)}{1+x}dx. \tag{25}$$

With the help from the existing expression for the CDF of the SA-SINR, the closed-form expression for the ergodic capacity can be provided in the following theorem.

Theorem 2: The employed dCDD-based CP-SC system achieves the ergodic capacity expressed by (26) expressed at the next page in i.i.d. frequency selective fading channels over the links from the Q interferers to CCD-RX.

Proof: See Appendix B. ∎

F. Ergodic Capacity Bound in Interference-Limited Region

In the noise-limited region, the PDF of the SINR can be approximated as

$$\gamma_{\text{SNR}}^{\text{NL}} \approx P_s\tilde{\alpha}_{h,\text{L}}\sum_{k=1}^{K}\|\tilde{\boldsymbol{h}}_{(M-K+k),\text{L}}\|^2 \tag{27}$$

with its PDF given by

$$f_{\gamma_{\text{SNR}}^{\text{NL}}}(x) = \frac{1}{\tilde{\alpha}_h}\Psi(M,K,N_h)\Bigg[\frac{B_1}{\Gamma(f)}\Big(\frac{x}{\tilde{\alpha}_h}\Big)^{f-1}e^{-\frac{x}{\tilde{\alpha}_h}} + \frac{B_2}{\Gamma(f)}\Big(\frac{x}{\beta\alpha}\Big)^{f-1}e^{-\frac{x}{\beta\tilde{\alpha}_h}}\Bigg]. \tag{28}$$

Thus, we can readily derive the ergodic capacity, which is defined by

$$C^{\text{NL}} = \frac{1}{\log(2)}\int_0^\infty \log(1+x)f_{\gamma_{\text{SNR}}^{\text{NL}}}(x)dx. \tag{29}$$

With some manipulations, we derive it as follows:

$$C^{\text{NL}} = \frac{\Psi(M,K,N_h)}{\log(2)}\Bigg[\frac{B_1}{\Gamma(f)}G_{3,1}^{2,3}\Big(\tilde{\alpha}_h\Big|\begin{array}{c}1-f,1,1\\1,0\end{array}\Big) + \frac{B_2\beta}{\Gamma(f)}G_{3,1}^{2,3}\Big(\beta\tilde{\alpha}_h\Big|\begin{array}{c}1-f,1,1\\1,0\end{array}\Big)\Bigg]. \tag{30}$$

Note that as SNR increases, we can see an increase in the ergodic capacity due to an increased received signal power. However, in the interference-limited region, it is upper bounded by the limit, which is derived in the following corollary.

Corollary 2: As SNR increases, the influence from the noise becomes negligible, so that the ergodic capacity is upper bounded by the limit, caused by interference, and is given by (31) at the next page.

Proof: We first use $F_{\gamma_{\text{SINR}}}^{\text{IL}}(x)$, which can be inferred from (22). And then by applying similar manipulations that we have used in the previous derivations, we can obtain an analytic expression for an upper bound on the ergodic capacity. ∎

Although *Corollary 2* verifies that C^{IL} is expressed by a combination of Meijer-G functions, it is constant with respect

$$C = \frac{\Psi(M,K,N_h)}{\log(2)}\Bigg[\sum_{l_a=0}^{f-1}\sum_{w=0}^{l_a}\binom{l_a}{w}\Bigg[\frac{B_1(1-\mathcal{F})}{\Gamma(N_{j,1})(\tilde{P}_J)^{N_{j,1}}}\frac{2R^{\epsilon_{\rm L}N_{j,1}}\tilde{\alpha}_h}{\epsilon_{\rm L}}$$
$$G_{1,0:1,1:2,2}^{1,0:1,1:2,1}\Big(\tilde{\alpha}_h,\tilde{\alpha}_h f_{f,1}\Big|\ \begin{matrix} w_1-l_a \\ \cdot \end{matrix}\ \Big|\ \begin{matrix} 0 \\ 0 \end{matrix}\ \Big|\ \begin{matrix} 1, f_{c,1} \\ f_{a,1}, w_1 \end{matrix}\ \Big) + \frac{\mathcal{F}}{\Gamma(N_{j,2})(\tilde{P}_J)^{N_{j,2}}}\frac{2R^{\epsilon_{\rm nL}N_{j,2}}\tilde{\alpha}_h}{\epsilon_{\rm nL}}$$
$$G_{1,0:1,1:2,2}^{1,0:1,1:2,1}\Big(\tilde{\alpha}_h,\tilde{\alpha}_h f_{f,2}\Big|\ \begin{matrix} w_2-l_a \\ \cdot \end{matrix}\ \Big|\ \begin{matrix} 0 \\ 0 \end{matrix}\ \Big|\ \begin{matrix} 1, f_{c,2} \\ f_{a,2}, w_2 \end{matrix}\ \Big)\Bigg] + \sum_{l_a=0}^{f-1}\sum_{w=0}^{l_a}\binom{l_a}{w}\Bigg[\frac{B_2(1-\mathcal{F})}{\Gamma(N_{j,1})(\tilde{P}_J)^{N_{j,1}}}\frac{2R^{\epsilon_{\rm L}N_{j,1}}\beta\tilde{\alpha}_h}{\epsilon_{\rm L}}$$
$$G_{1,0:1,1:2,2}^{1,0:1,1:2,1}\Big(\beta\tilde{\alpha}_h,\beta\tilde{\alpha}_h f_{f,3}\Big|\ \begin{matrix} w_1-l_a \\ \cdot \end{matrix}\ \Big|\ \begin{matrix} 0 \\ 0 \end{matrix}\ \Big|\ \begin{matrix} 1, f_{c,1} \\ f_{a,1}, w_1 \end{matrix}\ \Big) + \frac{\mathcal{F}}{\Gamma(N_{j,2})(\tilde{P}_J)^{N_{j,2}}}\frac{2R^{\epsilon_{\rm nL}N_{j,2}}\beta\tilde{\alpha}_h}{\epsilon_{\rm nL}}$$
$$G_{1,0:1,1:2,2}^{1,0:1,1:2,1}\Big(\beta\tilde{\alpha}_h,\beta\tilde{\alpha}_h f_{f,4}\Big|\ \begin{matrix} w_2-l_a \\ \cdot \end{matrix}\ \Big|\ \begin{matrix} 0 \\ 0 \end{matrix}\ \Big|\ \begin{matrix} 1, f_{c,2} \\ f_{a,2}, w_2 \end{matrix}\ \Big)\Bigg]\Bigg]. \tag{26}$$

$$C^{\rm IL} = \frac{\Psi(M,K,N_h)}{\log(2)}\Bigg[\sum_{l_a=0}^{f-1}\frac{B_1}{\Gamma(l_a+1)}\Bigg[\frac{(1-\mathcal{F})\Gamma(l_a+N_{j,1})}{\Gamma(N_{j,1})(P_J)^{N_{j,1}}}\frac{2R^{\epsilon_{\rm L}N_{j,1}}(\tilde{\alpha}_h)^{N_{j,1}}}{\epsilon_{\rm L}N_{j,1}+2}\frac{N_{j,1}+2/\epsilon_{\rm L}}{\Gamma(l_a+N_{j,1})}$$
$$G_{3,3}^{3,2}\Big(f_{f,1}\Big|\ \begin{matrix} 1, N_{j,1}, 1+N_{j,1}+2/\epsilon_{\rm L} \\ N_{j,1}+2/\epsilon_{\rm L}, l_a+N_{j,1}, N_{j,1} \end{matrix}\ \Big) + \frac{\mathcal{F}\Gamma(l_a+N_{j,2})}{\Gamma(N_{j,2})(P_J)^{N_{j,2}}}\frac{2R^{\epsilon_{\rm nL}N_{j,2}}(\tilde{\alpha}_h)^{N_{j,2}}}{\epsilon_{\rm nL}N_{j,2}+2}$$
$$G_{3,3}^{3,2}\Big(f_{f,2}\Big|\ \begin{matrix} 1, N_{j,2}, 1+N_{j,2}+2/\epsilon_{\rm nL} \\ N_{j,2}+2/\epsilon_{\rm nL}, l_a+N_{j,2}, N_{j,2} \end{matrix}\ \Big)\Bigg] +$$
$$\sum_{l_a=0}^{f-1}\frac{B_2}{\Gamma(l_a+1)}\Bigg[\frac{(1-\mathcal{F})\Gamma(l_a+N_{j,1})}{\Gamma(N_{j,1})(P_J)^{N_{j,1}}}\frac{2R^{\epsilon_{\rm L}N_{j,1}}(\beta\tilde{\alpha}_h)^{N_{j,1}}}{\epsilon_{\rm L}N_{j,1}+2}\frac{N_{j,1}+2/\epsilon_{\rm L}}{\Gamma(l_a+N_{j,1})}$$
$$G_{3,3}^{3,2}\Big(f_{f,3}\Big|\ \begin{matrix} 1, N_{j,1}, 1+N_{j,1}+2/\epsilon_{\rm L} \\ N_{j,1}+2/\epsilon_{\rm L}, l_a+N_{j,1}, N_{j,1} \end{matrix}\ \Big) + \frac{\mathcal{F}\Gamma(l_a+N_{j,2})}{\Gamma(N_{j,2})(P_J)^{N_{j,2}}}\frac{2R^{\epsilon_{\rm nL}N_{j,2}}(\beta\tilde{\alpha}_h)^{N_{j,2}}}{\epsilon_{\rm nL}N_{j,2}+2}$$
$$G_{3,3}^{3,2}\Big(f_{f,4}\Big|\ \begin{matrix} 1, N_{j,2}, 1+N_{j,2}+2/\epsilon_{\rm nL} \\ N_{j,2}+2/\epsilon_{\rm nL}, l_a+N_{j,2}, N_{j,2} \end{matrix}\ \Big)\Bigg]\Bigg]. \tag{31}$$

to the noise power. Other parameters, such as the degrees of RRH cooperation, number of multipath components, number of interferers, interference power, time-share factor for LoS and nLoS paths, and pathloss exponent jointly influence the magnitude of $C^{\rm IL}$.

IV. Simulations

In the simulations, we assume that

- $B = 192$ and $N_p = 64$, so that $K = 3$ is the maximum number of RRH for dCDD operation.
- Quadrature phase-shift keying (QPSK) modulation is used.
- Path-loss exponents are respectively assumed to be $\epsilon_{\rm L} = 2.09$, and $\epsilon_{\rm nL} = 3.75$, for LoS and nLoS paths [23].
- The transmission power is assumed to be $P_s = 1$ at the all RRHs.
- As a particular example, we assume a fixed number of multipath componenets over the interfering channels as $N_{j,\rm L} = 2$ and $N_{j,\rm nL} = 3$.
- CDD-RX is placed at the center of a circular shaped communication range of radius R. The extended radius is denoted by R_Δ.

The curves obtained via link-level simulations are denoted by **Ex**. Analytical performance curves are denoted by **An**. The SNR threshold causing an outage is fixed at $o_{\rm th} = 1$ dB.

A. Outage Probability

In Fig. 3, we verify the derivation for the outage probability for various cases. We assume $M = 3$ RRHs in the system, and $K = 3$ RRHs at maximum are selected for dCDD operation. We can observe from this figure that as K increases a lower outage probability can be obtained due to an increase in the received signal power at the CDD-RX. In addition, P_J is one of the key parameters that determines the outage probability. For various values of P_J and different degrees of RRH cooperation, we can see a good matching between the exact outage probability and that of the analytic derivation.

In Fig. 4, we investigate the effect of R_Δ on the outage probability. For fixed values of $(M = 3, N_h = 2, N_{j,\rm L} = 2, N_{j,\rm nL} = 3, P_J = -20$ dB$, \mathcal{F} = 0.6)$, we jointly investigate the effects of K, Q, and R_Δ on the outage probability. We can see that up to $R_\Delta = 9R$, the extended radius R_Δ does not impact the accuracy of the derivation. In addition, as Q increases, a higher outage probability is obtained due to the presence of a stronger interference. With the same other

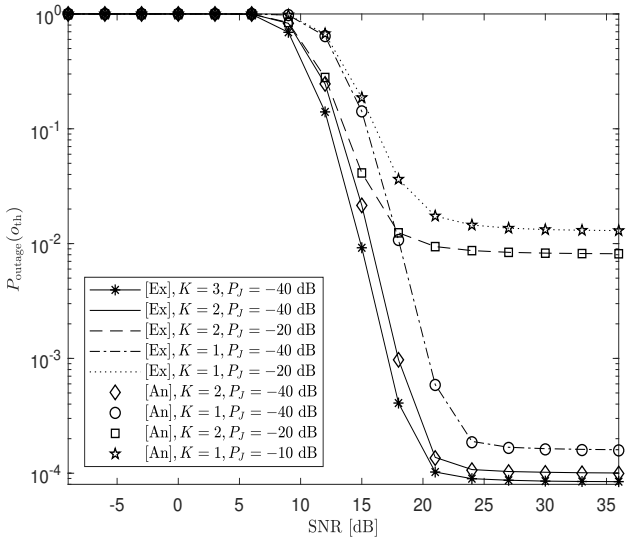

Fig. 3. Outage probability for various scenarios at a fixed value of ($Q = 5, \mathcal{F} = 1.0, N_h = 2$).

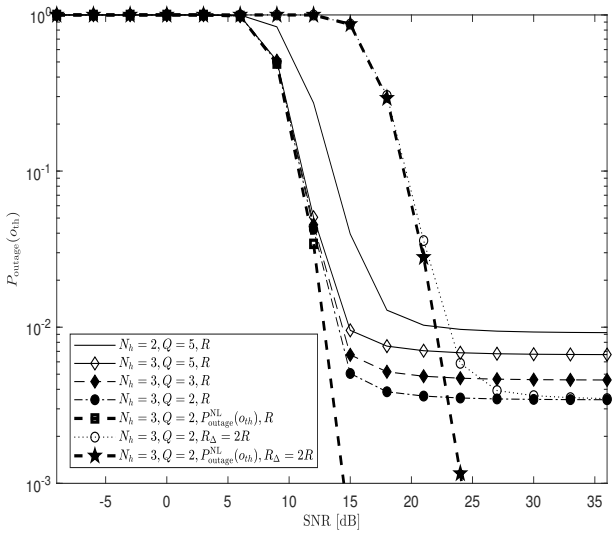

Fig. 5. Outage probability for various scenarios at a fixed value of $\mathcal{F} = 0.6$.

simulation parameters except K, a lower outage probability can be achievable as K increases since the received signal power can be increased at the CDD-RX.

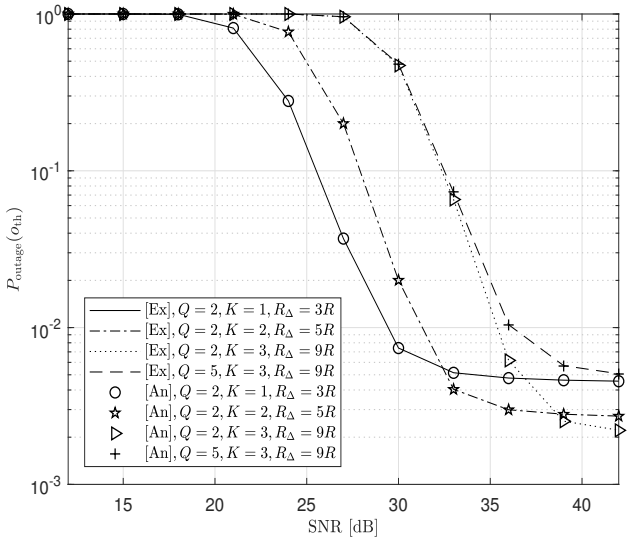

Fig. 4. Outage probability for various values of R_Δ, Q, and K.

Thus, in the sequel, we will mainly use the analytical expression to evaluate the performance of the proposed system. However, as SNR increases, the outage probability approaches the outage probability floor. This will be investigated next.

In Fig. 5, at a fixed value of ($M = 3, K = 2, P_J = -20$ dB$, \mathcal{F} = 0.6$), we investigate the impact of several system parameters on the outage probability, for example, the number of interfereres, Q, number of multipath components, N_h, and different size of the communication range, R. As SNR increases, the effect from the noise becomes disappear, so that the system enters interference-limited region. As verified by Corollary 1, in interference-limited region, the outage probability is limited by the outage floor determined by system parameters. We can see a lower outage probability as either of RRH cooperation, the number of multipath channel elements over the RRHs to the CDD-RX, or the communication range, R, increases. Also, as either of the number of interferers or a power allocated to interferers decreases, a lower outage probability is obtained. Especially, the size of the communication range is more significant than other parameters due to the path-loss exponent. In addition, in the noise-limited region, diversity gain is $G_d = MN_h$, so that it is independent of Q and R. By comparing $P^{\text{NL}}_{\text{outage}}(o_{\text{th}})$ with other curves, we can justify this diversity gain.

To investigate the diversity gain in detail, we use various values of $\mathcal{F}$ and K for the system with $M = 3$, $Q = 5$, $N_h = 2$, $N_{j,\text{L}} = 3$, and $N_{j,\text{nL}} = 3$. At a fixed value of $P_J = -20$ dB, outage probabilities are plotted in the $\log_{10} - \log_{10}$ scale.

From Fig. 6, we can summarize the observation as follows:

- Two distinctive regions, i.e., noise-limited region and interference-limited region are noticeable.
- In the interference-limited region, the outage probability is almost identical to $P^{\text{IL}}_{\text{outage}}(o_{\text{th}})$, and the slope of the outage probability becomes zero. That is, the maximum diversity gain is not achievable.
- Diversity gain, $G_d = MN_h$, is achievable only in the noise-limited region. By measuring the slopes using $-\log_{10}(P^{\text{NL}}_{\text{outage}}(o_{\text{th}}))$, we can see that $G_d \approx 6$ for $M = 3$ and $N_h = 2$. The diversity gain achievable by dCDD is

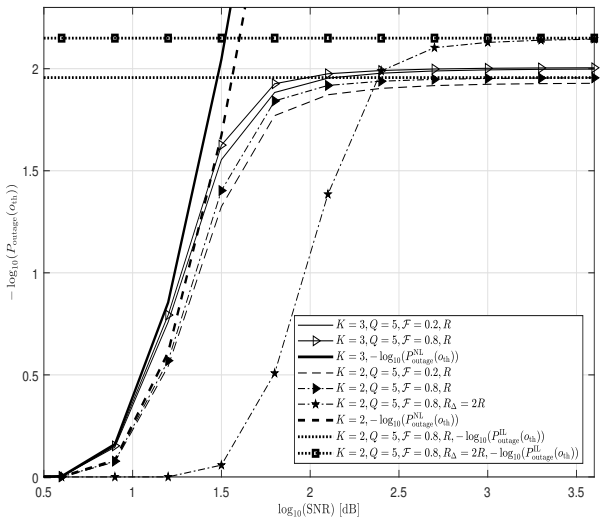

Fig. 6. Outage probability for various scenarios.

independent of the number of RRHs for CDD operation. Comparing $-\log_{10}(P^{\mathrm{NL}}_{\mathrm{outage}}(o_{\mathrm{th}}))$ with $K=2$ and $K=3$, a same slope is measured. The number of interferers has no effect on the diversity gain, whereas it affects the outage probability floor. As it increases, it lowers the the outage probability floor. Thus, the diversity gain depends on the total number of RRHs in the system. As the communication range, R, increases, a lower outage probability floor, is obtained. As R increases, channel power from the interferers and RRHs to the CDD-Rx is decreasing. However, the loss from the desired channel power loss is more critical.

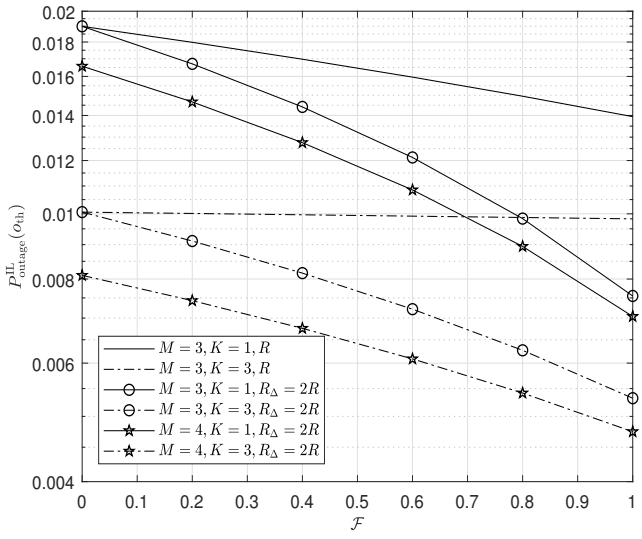

Fig. 7. Outage probability in interference-limited region for various scenarios.

Fig. 7 shows the outage probability in the interference-limited region for various values of M, K, and R. We used fixed values of $N_h=2$, $N_{j,\mathrm{L}}=3$, and $N_{j,\mathrm{nL}}=3$. In general, as $\mathcal{F}$ increases, a lower $P^{\mathrm{IL}}_{\mathrm{outage}}(o_{\mathrm{th}})$ is obtained. In addition, as R increases, a lower $P^{\mathrm{IL}}_{\mathrm{outage}}(o_{\mathrm{th}})$ is obtained. At the same degrees of RRH cooperation, a more number of RRHs results in a lower $P^{\mathrm{IL}}_{\mathrm{outage}}(o_{\mathrm{th}})$. As $\mathcal{F}$ increases, NLoS path has a more selection in time than LoS path. Since the nLoS path loss exponent is bigger than that of the LoS path, interference power will be decreased. Thus, at the same condition with other parameters, this results in a lower outage probability.

In Fig. 8, we examine the accuracy of the approximation made in (27) for the outage probability. In this simulation, we use the fixed values of $(M=3, N_h=2, \mathrm{SNR}=33\ \mathrm{dB}, \mathcal{F}=0.6)$. From this figure, we can observe that the approximation

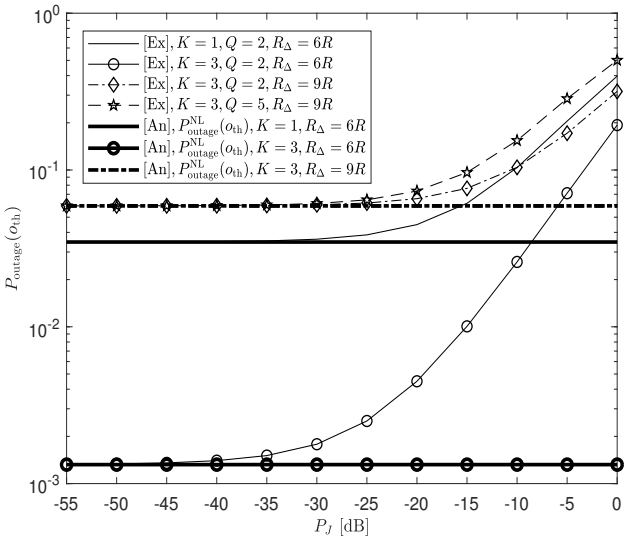

Fig. 8. Outage probability for various values of R_Δ, K, and Q.

accuracy mainly depends on the outage probability in the noise-limited region. That is, P_J is proportional to the outage probability. For example, since $K=3$ with $R_\Delta=6$ provides a lower outage probability than that of $K=3$ with $R_\Delta=9$, this requires 15 dB less P_J to achieve a very accurate approximation. Similarly, $K=3$ with $Q=2$ and $R_\Delta=6$ requires 5 dB less P_J to achieve a very accurate approximation than that of $K=3$ with $Q=5$ and $R_\Delta=6$. Thus, the size of the extended radius, R_Δ, number of RRHs for dCDD, K, number of multipath components, and number of interferers, Q, jointly determine P_J in achieving an accurate approximation.

B. Ergodic Capacity

We investigate the impact of several parameters on the ergodic capacity. In Fig. 9, we first compare the analytic ergodic capacity with its corresponding exact ergodic capacity for different values of $\mathcal{F}$. For a fixed $(M=3, K=1, Q=5, P_J=-20\ \mathrm{dB})$, we can see a good matching between them. As SNR increases, the ergodic capacity approaches the limit or ceiling, denoted by C^{IL}. As in the outage probability, we can see different results in two distinct regions. They are

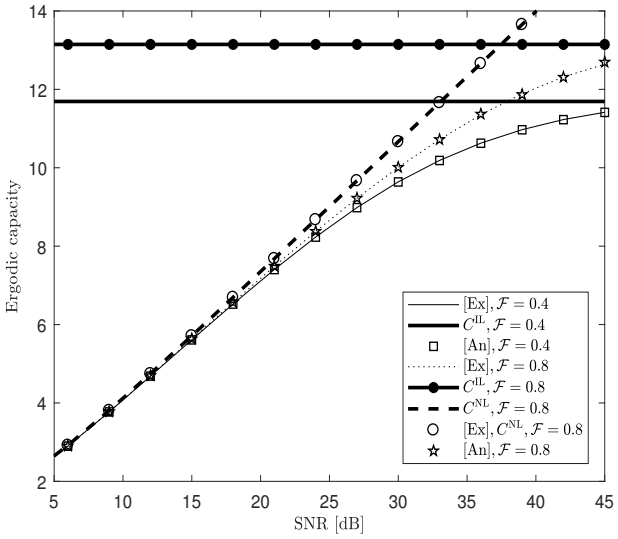

Fig. 9. Ergodic capacity for a different value of $\mathcal{F}$ at a fixed value of $(M = 3, N_h = 2, K = 1, Q = 5, P_J = -20$ dB).

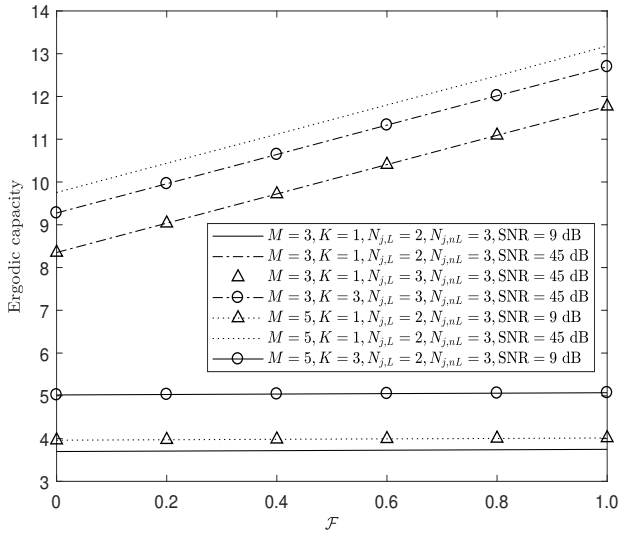

Fig. 11. Ergodic capacity for a different value of $\mathcal{F}$ at a fixed value of $(M = 3, N_h = 2, Q = 2, P_J = -10$ dB).

respectively expressed by C^{NL} and C^{IL}. The ergodic capacity follows C^{NL} at first in a lower SNR region, but it is finally upper bounded by C^{IL}. In the sequel, we will mainly use the exact ergodic capacity in the forthcoming ergodic capacity analysis.

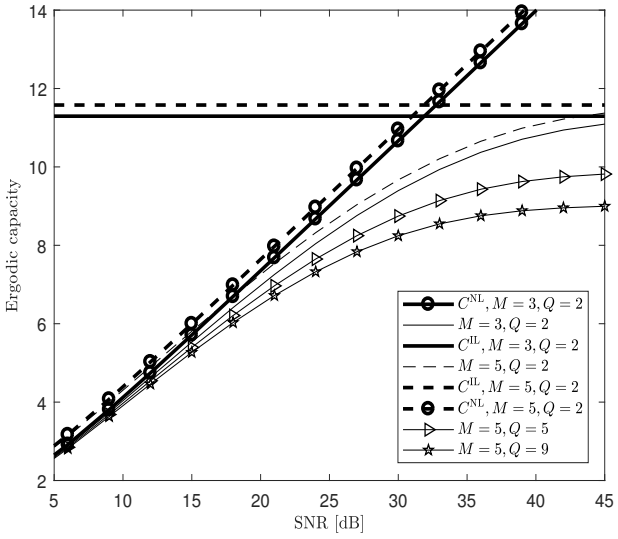

Fig. 10. Ergodic capacity for various values of M and Q at a fixed value of $(N_h = 2, K = 1, \mathcal{F} = 0.2, P_J = -10$ dB).

In Fig. 10, we investigate the effect of the total number of RRHs, M, and the number of interferers, Q, in the system at a fixed value of $(N_h = 2, K = 1, \mathcal{F} = 0.2, P_J = -10$ dB). From this figure, we can see that a more number of RRHs in the system results in a larger ergodic capacity and ergodic capacity limit. A more number of interferers results in a lower ergodic capacity.

In Fig. 11, we investigate the impact of the number of RRHs, M, number of multipath elements for interfering channels, $(N_{j,\mathrm{L}}, N_{j,\mathrm{nL}})$, SNR, and RRH cooperation, K, as a function of $\mathcal{F}$. At a lower SNR region, the effect of $\mathcal{F}$ does not make significant differences in the ergodic capacity. However, its effect becomes significant as the SNR increases. In this particular scenario, the number of multipath elements, $(N_{j,\mathrm{L}}, N_{j,\mathrm{nL}})$, makes a minor difference, for example, $(N_{j,\mathrm{L}} = 2, N_{j,\mathrm{nL}} = 3)$ vs. $(N_{j,\mathrm{L}} = 3, N_{j,\mathrm{nL}} = 3)$. At the same SNR, a more RRH cooperation results in a higher ergodic capacity. Since dCDD applies the opportunistic RRH selection using the channel magnitude, a more number of RRHs results in a higher ergodic. In general, as $\mathcal{F}$ increases, a higher ergodic capacity is obtained since a more fraction of time select nLoS path whose pathloss exponent is bigger than that of the LoS path.

V. Conclusions

In this paper, we have investigated the effects of spatially distributed interferers and coexisting LoS and nLoS paths on the outage probability and ergodic capacity of a single carrier system that applies dCDD. For this more realistic channel environment, we have derived the SA-CDF of the SINR, and then derived the closed-form expressions for the outage probability and ergodic capacity. From the derivations and system level simulations, we have verified the existence of two distinguishable regions, noise-limited and interference-limited regions, in which different performance behaviors occurred. Especially, only in the noise-limited region, a desirable diversity gain is achievable depending on the total number of RRHs and the number of multipath components. In contrast, performance limits in the outage probability, and ergodic capacity are intrinsic in the interference-limited region. Thus, the maximum diversity gain is not achievable. It can be shown that the most efficient way to improve the performance in

the interference-limited case is to use as many as RRHs for dCDD operation whenever they are supported by dCDD. For a fixed frequency selective fading channel environment, this can be possible by using a larger size of the symbol block for transmissions.

Appendix A: Derivation of Theorem 1

If we express the upper incomplete gamma function in terms of series expansions [31, eq. (8.352.2)], then we can see that $F_S(x)$ is proportional to a term $e^{-\tilde{a}x}x^{\tilde{m}}$ for $\tilde{a} \in \mathbb{R}_+$ and $\tilde{m} \in \mathbb{N}_0$, we will mainly focus on the computation related with this in the sequel.

$$\begin{aligned} F_S((J+1)x|\mathbb{A}_j) &\propto x^{\tilde{m}}e^{-\tilde{a}(J+1)x}(J+1)^{\tilde{m}} \\ &= x^{\tilde{m}}\sum_{q=0}^{\tilde{m}}\binom{\tilde{m}}{q}e^{-\tilde{a}(J+1)x}J^q. \end{aligned} \tag{A.1}$$

The PDF of J is given by

$$\begin{aligned} f_J(x) = (1-\mathcal{F})&\frac{e^{-x/\tilde{P}_J\alpha_{j_{,\mathrm{L}}}}x^{QN_{j,\mathrm{L}}-1}}{\Gamma(QN_{j,\mathrm{L}})(\tilde{P}_J\alpha_{j_{,\mathrm{L}}})^{QN_{j,\mathrm{L}}}} \\ &+\mathcal{F}\frac{e^{-x/\tilde{P}_J\alpha_{j_{,\mathrm{nL}}}}x^{QN_{j,\mathrm{nL}}-1}}{\Gamma(QN_{j,\mathrm{nL}})(\tilde{P}_{J,}\alpha_{j_{,\mathrm{nL}}})^{QN_{j,\mathrm{nL}}}}. \end{aligned} \tag{A.2}$$

Applying (A.2), $E_{\mathbb{X}_j}\{F_S((J+1)x|\mathbb{A}_j)\}$ is given by (A.3). In (A.3), K_1 and K_2 are respectively given by

$$K_1 = \Gamma(q+QN_{j,\mathrm{L}})\left(\tilde{a}x+\frac{1}{\tilde{P}_J\alpha_{j_{,\mathrm{L}}}}\right)^{-(q+QN_{j,\mathrm{L}})}, \tag{A.4}$$

$$K_2 = \Gamma(q+QN_{j,\mathrm{nL}})\left(\tilde{a}x+\frac{1}{\tilde{P}_J\alpha_{j_{,\mathrm{nL}}}}\right)^{-(q+QN_{j,\mathrm{nL}})}. \tag{A.5}$$

Thus, the terms inside of brackets $[\cdot]$ in (A.3) are evaluated as

$$\begin{aligned} \Big[\,\cdot\,\Big] = &\frac{(1-\mathcal{F})\Gamma(q+QN_{j,\mathrm{L}})}{\Gamma(QN_{j,\mathrm{L}})(\tilde{P}_J\alpha_{j_{,\mathrm{L}}})^{QN_{j,\mathrm{L}}}}\left(\tilde{a}x+\frac{1}{\tilde{P}_J\alpha_{j_{,\mathrm{L}}}}\right)^{-(q+QN_{j,\mathrm{L}})} \\ &+\frac{\mathcal{F}\Gamma(q+QN_{j,\mathrm{nL}})}{\Gamma(QN_{j,\mathrm{nL}})(\tilde{P}_J\alpha_{j_{,\mathrm{nL}}})^{QN_{j,\mathrm{nL}}}} \\ &\left(\tilde{a}x+\frac{1}{\tilde{P}_J\alpha_{j_{,\mathrm{nL}}}}\right)^{-(q+QN_{j,\mathrm{nL}})} \end{aligned} \tag{A.6}$$

which is alternatively expressed as follows by applying expressions for $\alpha_{j_{t,\mathrm{L}}}$ and $\alpha_{j_{t,\mathrm{nL}}}$

$$\begin{aligned} \Big[\,\cdot\,\Big] = &\frac{(1-\mathcal{F})\Gamma(q+QN_{j,\mathrm{L}})(d)^{QN_{j,\mathrm{L}}\epsilon_{\mathrm{L}}}}{\Gamma(QN_{j,\mathrm{L}})(\tilde{P}_J)^{QN_{j,\mathrm{L}}}} \\ &\left(\tilde{a}x+\frac{(d)^{\epsilon_{\mathrm{L}}}}{\tilde{P}_J}\right)^{(q+QN_{j,\mathrm{L}})} \\ &+\frac{\mathcal{F}\Gamma(q+QN_{j,\mathrm{nL}})(d)^{QN_{j,\mathrm{nL}}\epsilon_{\mathrm{nL}}}}{\Gamma(QN_{j,\mathrm{nL}})(\tilde{P}_J)^{QN_{j,\mathrm{nL}}}} \\ &\left(\tilde{a}x+\frac{(d)^{\epsilon_{\mathrm{nL}}}}{\tilde{P}_J}\right)^{-(q+QN_{j,\mathrm{nL}})}. \end{aligned} \tag{A.7}$$

For the stochastic random location of interferers in the interest area, PDFs of $y_1 \triangleq (d)^{\epsilon_{\mathrm{L}}}$ and $y_2 \triangleq (d)^{\epsilon_{\mathrm{nL}}}$ are respectively given by

$$\begin{aligned} f_{y_1}(x) &= \frac{2x^{2/\epsilon_{\mathrm{L}}}-1}{\epsilon_{\mathrm{L}}R^2} \text{ and} \\ f_{y_2}(x) &= \frac{2x^{2/\epsilon_{\mathrm{nL}}}-1}{\epsilon_{\mathrm{nL}}R^2}, \text{for } 0<x<2R. \end{aligned} \tag{A.8}$$

Thus, we can compute $E_{\mathbb{A}_j}\{E_{\mathbb{X}_j}\{F_S((J+1)x|\mathbb{A}_j)\}\}$ as in (A.9). After some manipulations, we can have (18).

Appendix B: Derivation of Theorem 2

We can see that the ergodic capacity is proportional to the definite integral containing

$$C \propto \int_0^\infty \frac{1}{1+x}e^{-\frac{x}{b}}x^{a-1}{}_2F_1\Big(f_a,q_j;f_c;-1/(f_fx)\Big)dx \tag{B.1}$$

where $e^{-\frac{x}{b}}x^{a-1}{}_2F_1\Big(f_a,q_j;f_c;-\frac{1}{f_fx}\Big)$ for $\{b,f_f\} \in \mathbb{R}_+$ and $\{a,q_j\} \in \mathbb{N}_0$. As far as we know, there is no solution of (B.1). To compute (B.1), we express the following functions of x in terms of Meijer-G functions [32, eqs. (07.34.03.0271.01),(07.34.16.0002.01),(07.34.03.0228.01), (07.23.26.0004.01)] as follows:

$$\begin{aligned} \frac{1}{1+x} &= G_{1,1}^{1,1}\Big(x\Big|\begin{array}{c}0\\0\end{array}\Big), \\ e^{-\frac{x}{b}} &= G_{0,1}^{1,0}\Big(x/b\Big|\begin{array}{c}\cdot\\0\end{array}\Big), \text{ and} \\ {}_2F_1\big(f_a,q_j;f_c;-\frac{1}{f_fx}\big) &= C_\Delta G_{2,2}^{2,1}\Big(f_fx\Big|\begin{array}{c}1,f_c\\f_a,q_j\end{array}\Big) \end{aligned} \tag{B.2}$$

where it is assumed that $f_c \neq -l, l \in \mathbb{N}_0$. In addition, we have defined $C_\Delta \triangleq \frac{\Gamma(f_a)}{\Gamma(q_j)\Gamma(f_c)}$. Using Meijer-G identities given in (B.2), (B.1) is rewritten as

$$\begin{aligned} C \propto C_\Delta \int_0^\infty &x^{a-1}G_{0,1}^{1,0}\Big(x/b\Big|\begin{array}{c}\cdot\\0\end{array}\Big)G_{1,1}^{1,1}\Big(x\Big|\begin{array}{c}0\\0\end{array}\Big) \\ &G_{2,2}^{2,1}\Big(f_fx\Big|\begin{array}{c}1,f_c\\f_a,q_j\end{array}\Big)dx \end{aligned} \tag{B.3}$$

which show an integral from three Meijer G-function. Using the generalized bivariate Meijer G-function [32, eq. (07.34.21.0081.01)] and [36, Eqs. (9)-(11)], (B.3) is derived as

$$\begin{aligned} C \propto &C_\Delta\big(b\big)^a \\ &G_{1,0:1,1:2,1}^{1,0:1,1:2,1}\Big(b,bf_f,\Big|\begin{array}{c|c|c}1-a & 1,1 & 1,f_c\\ \cdot & 1,0 & f_a,q_j\end{array}\Big). \end{aligned} \tag{B.4}$$

Using (B.4), we can obtain (26).

References

[1] J. K. Cavers, "Single-user and multiuser adaptive maximal ratio transmission for Rayleigh channels," *IEEE Trans. Veh. Technol.*, vol. 49, no. 6, pp. 2043–2050, Nov. 2000.

[2] T. K. Y. Lo, "Maximum ratio transmission," *IEEE Trans. Commun.*, vol. 47, no. 10, pp. 1458–1461, Oct. 1999.

[3] K. J. Kim, T. Khan, and P. Orlik, "Performance analysis of cooperative systems with unreliable backhauls and selection combining," *IEEE Trans. Veh. Technol.*, vol. 66, no. 3, pp. 2448–2461, Mar. 2017.

[4] J. N. Laneman and G. W. Wornell, "Energy-efficient antenna sharing and relaying for wireless networks," in *Proc. IEEE Wireless Communications and Networking Conf.*, Chicago, IL, Oct. 2000, pp. 7–12.

$$E_{\mathbb{X}_j}\{F_S((J+1)x|\mathbb{A}_j)\} \propto x^{\tilde{m}} \sum_{q=0}^{\tilde{m}} \binom{\tilde{m}}{q} e^{-\tilde{a}x} \Bigg[\frac{(1-\mathcal{F})}{\Gamma(QN_{j,\mathrm{L}})(\tilde{P}_J \alpha_{j,\mathrm{L}})^{QN_{j,\mathrm{L}}}} \underbrace{\int_0^\infty e^{-y(\tilde{a}x+1/\tilde{P}_J\alpha_{j,\mathrm{L}})} y^{q+QN_{j,\mathrm{L}}-1} dy}_{K_1} + \frac{\mathcal{F}}{\Gamma(QN_{j,\mathrm{nL}})(\tilde{P}_J \alpha_{j,\mathrm{nL}})^{QN_{j,\mathrm{nL}}}} \underbrace{\int_0^\infty e^{-y(\tilde{a}x+1/\tilde{P}_J\alpha_{j,\mathrm{nL}})} y^{p+QN_{j,\mathrm{nL}}-1} dy}_{K_2} \Bigg]. \tag{A.3}$$

$$\begin{aligned} E_{\mathbb{A}_j}\{E_{\mathbb{X}_j}\{F_S((J+1)x|\mathbb{A}_j)\}\} \propto x^{\tilde{m}} e^{-\tilde{a}x} \Bigg[& \frac{(1-\mathcal{F})\Gamma(q+QN_{j,\mathrm{L}})}{\Gamma(QN_{j,\mathrm{L}})(\tilde{P}_J)^{QN_{j,\mathrm{L}}}} \frac{2(R)^{(\epsilon_{\mathrm{L}} QN_{j,\mathrm{L}}+2)}(\tilde{a}x)^{-q-QN_{j,\mathrm{L}}}}{\epsilon_{\mathrm{L}} R^2 (QN_{j,\mathrm{L}}+2/\epsilon_{\mathrm{L}})} \\ & {}_2F_1\Big(QN_{j,\mathrm{L}}+2/\epsilon_{\mathrm{L}}, q+QN_{j,\mathrm{L}}; QN_{j,\mathrm{L}}+2/\epsilon_{\mathrm{L}}+1; -R^{\epsilon_{\mathrm{L}}}/(\tilde{P}_J\tilde{a}x)\Big) + \\ & \frac{\mathcal{F}\Gamma(q+QN_{j,\mathrm{nL}})}{\Gamma(QN_{j,\mathrm{nL}})(\tilde{P}_J)^{QN_{j,\mathrm{nL}}}} \frac{2(R)^{(\epsilon_{\mathrm{nL}} QN_{j,\mathrm{nL}}+2)}(\tilde{a}x)^{-q-QN_{j,\mathrm{nL}}}}{\epsilon_{\mathrm{nL}} R^2 (QN_{j,\mathrm{nL}}+2/\epsilon_{\mathrm{nL}})} \\ & {}_2F_1\Big(QN_{j,\mathrm{nL}}+2/\epsilon_{\mathrm{nL}}, q+QN_{j,\mathrm{nL}}; QN_{j,\mathrm{nL}}+2/\epsilon_{\mathrm{nL}}+1; -R^{\epsilon_{\mathrm{nL}}}/(\tilde{P}_J\tilde{a}x)\Big) \Bigg]. \end{aligned} \tag{A.9}$$

[5] M. O. Astal and A. M. Abu-Hudrouss, "SIC detector for 4 relay distributed space-time block coding under quasi-synchronization," *IEEE Commun. Lett.*, vol. 15, no. 10, pp. 1056–1058, Oct. 2011.

[6] R. Tanbourgi, S. Singh, J. G. Andrew, and F. K. Jondral, "A tractable model for non-coherent joint-transmission base station cooperation," *IEEE Trans. Wireless Commun.*, vol. 13, no. 9, pp. 4959 –4973, Sep. 2014.

[7] K. J. Kim, P. V. Orlik, and T. A. Khan, "Performance analysis of finite-sized co-operative systems with unreliable backhauls," *IEEE Trans. Wireless Commun.*, vol. 15, no. 7, pp. 5001–5015, Jul. 2016.

[8] IEEE, "Wireless LAN medium access control (MAC) and physical layer (PHY) specifications–Amendment 4: Enhancements for very high throughput for operation in bands below 6 GHz," *IEEE Standard 802.11ac-2013, Part 11*, 2009.

[9] ——, "Wireless LAN medium access control (MAC) and physical layer (PHY) specifications - Amendment 5: Enhancements for higher throughput," *IEEE Standard 802.11n-2009, Part 11*, 2009.

[10] 3GPP, Technical Specification Group Radio Access Network, "Evolved universal terrestrial radio access (E-UTRA): Physical channels and modulation (release 8)," *3GPP TS 36.211 V8.9.0 (2009-12) Technical Specification*, Mar. 2009.

[11] IEEE P802.11ad/D0.1, "Wireless LAN medium access control (MAC) and physical layer (PHY) specifications: Enhancements for very high throughput in the 60GHz band," Jun. 2010.

[12] S. Kato, H. Harada, R. Funada, T. Baykas, C. S. Sum, J. Wang, and M. A. Rahman, "Single carrier transmission for multi-gigabit 60-GHz WPAN systems," *IEEE J. Sel. Areas Commun.*, vol. 27, no. 8, pp. 1466–1478, Oct. 2009.

[13] Y.-C. Liang, W. S. Leon, Y. Zeng, and C. Xu, "Design of cyclic delay deievsity for single carrier cyclic prefix (sccp) transmissions with block-iterative GDFE (BI-GDFE) receiver," *IEEE Trans. Wireless Commun.*, vol. 7, no. 2, pp. 677–684, Feb. 2008.

[14] A. H. Mehana and A. Nosratinia, "Single-carrier frequency-domain equalizer with multi-antenna transmit diversity," *IEEE Trans. Wireless Commun.*, vol. 12, pp. 388–397, Jan. 2013.

[15] Q. Li, Q. Yan, K. C. Keh, K. H. Li, and Y. Hu, "A multi-relay-selection scheme with cyclic delay diversity," *IEEE Commun. Lett.*, vol. 17, no. 2, pp. 349–352, Feb. 2013.

[16] U.-K. Kwon and G.-H. Im, "Cyclic delay diversity with frequency domain Turbo equalization for uplink fast fading channels," *IEEE Commun. Lett.*, vol. 13, no. 3, pp. 184–186, Mar. 2009.

[17] K. J. Kim, M. D. Renzo, H. Liu, P. V. Orlik, and H. V. Poor, "Performance analysis of distributed single carrier systems with distributed cyclic delay diversity," *IEEE Trans. Commun.*, vol. 65, no. 12, pp. 5514 – 5528, Dec. 2017.

[18] K. J. Kim and T. A. Tsiftsis, "On the performance of cyclic prefix-based single-carrier cooperative diversity systems with best relay selection," *IEEE Trans. Wireless Commun.*, vol. 10, no. 4, pp. 1269–1279, Apr. 2011.

[19] K. J. Kim, T. A. Tsiftsis, and H. V. Poor, "Power allocation in cyclic prefixed single-carrier relaying systems," *IEEE Trans. Wireless Commun.*, vol. 10, no. 7, pp. 2297–2305, Jul. 2011.

[20] X. Zhang and J. G. Andrew, "Downlink cellular network analysis with multi-slope path loss models," *IEEE Trans. Commun.*, vol. 63, no. 5, pp. 1881–1894, May 2015.

[21] T. Bai, R. Vaze, and R. W. Heath, "Analysis of blockage effects on urban cellular networks," *IEEE Trans. Wireless Commun.*, vol. 9, no. 13, pp. 5070–5083, Sep. 2014.

[22] M. Ding, P. Wang, D. Lopez-Perez, G. Mao, and Z. Lin, "Performance impact of LoS and NLoS transmissions in dense cellular networks," *IEEE Trans. Wireless Commun.*, vol. 15, no. 3, pp. 2365–2380, Mar. 2016.

[23] 3GPP, TR 36.828 (V11.0.0), "Further enhancements to lte time division duplex (TDD) for downlink-uplink (DL-UL) interference management and traffic adaptation," Jun. 2012.

[24] C. M. Lo and W. H. Lam, "Performance of generalized selection combining for mobile radio communications with mixed cochannel interferers," *IEEE Trans. Veh. Technol.*, vol. 51, no. 1, pp. 114–121, Jan. 2002.

[25] I. Atzeni, J. Arnau, and M. Kountouris, "Downlink cellular network analysis with LOS/NLOS propagation and elevated base stations," *IEEE Trans. Wireless Commun.*, vol. 17, no. 1, pp. 142–156, Jan. 2018.

[26] B. Yang, G. Mao, M. Ding, X. Ge, and X. Tao, "Dense small cell networks: From noise-limited to dense interference-limited," *IEEE Trans. Veh. Technol.*, vol. PP, no. 99, pp. 1–1, 2018.

[27] Y. Zeng and T. S. Ng, "Pilot cyclic prefixed single carrier communication: channel estimation and equalization," *IEEE Signal Process. Lett.*, vol. 12, no. 1, pp. 56–59, Jan. 2005.

[28] F. Gao, A. Nallanathan, and C. Tellambura, "Blind channel estimation for cyclic-prefixed single-carrier systems by exploiting real symbol characteristics," *IEEE Trans. Veh. Technol.*, vol. 56, no. 5, pp. 2487–2498, Sept. 2007.

[29] K. J. Kim, Y. Yue, R. A. Iltis, and J. D. Gibson, "A QRD-M/Kalman Filter-based detection and channel estimation algorithm for MIMO-OFDM systems," *IEEE Trans. Wireless Commun.*, vol. 4, pp. 710–721, Mar. 2005.

[30] K. J. Kim and T. A. Tsiftsis, "Performance analysis of QRD-based cyclically prefixed single-carrier transmissions with opportunistic scheduling," *IEEE Trans. Veh. Technol.*, vol. 60, no. 1, pp. 328–333, Jan. 2011.

[31] I. S. Gradshteyn and I. M. Ryzhik, *Table of Integrals, Series, and Products*. New York: Academic Press, 2007.

[32] Wolfman research inc. [Online]. Available: http://functions.wolfman.com

[33] I. Shafique, S. Al-Ahmadi, F. Yilmaz, M.-S. Alouini, and H. Yanikomeroglu, "A new formula for the BER of binary modulations with dual-branch selection over generalized-K composite fading channels," *IEEE Trans. Commun.*, vol. 59, no. 10, pp. 2654–2658, Oct. 2011.

[34] H. Chergui, M. Benjillali, and S. Saoudi, "Performance analysis of project-and-forward relaying in mixed MIMO-pinhole and Rayleigh dual-hop channel," *IEEE Commun. Lett.*, vol. 20, no. 3, pp. 610–613, Mar. 2016.

[35] H. A. Suraweera, P. J. Smith, and M. Shafi, "Capacity limits and performance analysis of cognitive radio with imperfect channel knowledge," *IEEE Trans. Veh. Technol.*, vol. 59, pp. 1811–1822, May 2010.

[36] C. Garca-Corrales, F. J. Caete, and J. F. Paris, "Capacity of κ-μ shadowed fading channels," *International Journal of Antennas and Propagation*, vol. 2014, 2014. [Online]. Available: http://dx.doi.org/10.1155/2014/975109